

# Disruption of sheetlike structures in Alfvénic turbulence by magnetic reconnection

A. Mallet<sup>1\*</sup>, A. A. Schekochihin<sup>2,3</sup>, B. D. G. Chandran<sup>1</sup>

<sup>1</sup>Space Science Center, University of New Hampshire, Durham, NH 03824, USA

<sup>2</sup>Rudolf Peierls Centre for Theoretical Physics, University of Oxford, Oxford OX1 3NP, United Kingdom

<sup>3</sup>Merton College, Oxford OX1 4JD, United Kingdom

27 November 2018

## ABSTRACT

We propose a mechanism whereby the intense, sheetlike structures naturally formed by dynamically aligning Alfvénic turbulence are destroyed by magnetic reconnection at a scale  $\hat{\lambda}_D$ , larger than the dissipation scale predicted by models of intermittent, dynamically aligning turbulence. The reconnection process proceeds in several stages: first, a linear tearing mode with  $N$  magnetic islands grows and saturates, and then the  $X$ -points between these islands collapse into secondary current sheets, which then reconnect until the original structure is destroyed. This effectively imposes an upper limit on the anisotropy of the structures within the perpendicular plane, which means that at scale  $\hat{\lambda}_D$  the turbulent dynamics change: at scales larger than  $\hat{\lambda}_D$ , the turbulence exhibits scale-dependent dynamic alignment and a spectral index approximately equal to  $-3/2$ , while at scales smaller than  $\hat{\lambda}_D$  the turbulent structures undergo a succession of disruptions due to the reconnection mechanism, limiting dynamic alignment, steepening the effective spectral index and changing the scaling of the final dissipation scale. The scaling of the transition scale  $\hat{\lambda}_D$  with the Lundquist (magnetic Reynolds) number  $S_{L_\perp}$  depends on the order of the statistics being considered, and on the specific model of intermittency; the transition between the two regimes in the energy spectrum is predicted at approximately  $\hat{\lambda}_D \sim S_{L_\perp}^{-0.6}$ . The final dissipation scale is at  $\hat{\lambda}_{\eta,\infty} \sim S_{L_\perp}^{-0.8}$ , and may be indistinguishable from the Kolmogorov scale for currently feasible numerical simulations.

**Key words:** MHD—turbulence—magnetic reconnection—solar wind

## 1 INTRODUCTION

Turbulence is thought to be important in many astrophysical situations, and is also measured directly by spacecraft in the solar wind (Bruno & Carbone 2013). In many situations, the system consists of an ionized plasma threaded by a strong mean magnetic field  $\mathbf{B}_0$ . In this case, the Alfvénically polarized fluctuations decouple from the compressive modes and satisfy the reduced magnetohydrodynamics (RMHD) equations (Strauss 1976), regardless of the collisionality of the plasma (Schekochihin et al. 2009). Written in terms of Elsasser (1950) variables  $\mathbf{z}_\perp^\pm = \mathbf{u}_\perp \pm \mathbf{b}_\perp$ , where  $\mathbf{u}_\perp$  and  $\mathbf{b}_\perp$  are the velocity and magnetic field (in velocity units) perturbations perpendicular to  $\mathbf{B}_0$ , these equations are

$$\partial_t \mathbf{z}_\perp^\pm \mp v_A \partial_z \mathbf{z}_\perp^\pm + \mathbf{z}_\perp^\pm \cdot \nabla_\perp \mathbf{z}_\perp^\pm = -\nabla_\perp p, \quad (1)$$

where the pressure  $p$  is obtained from the solenoidality condition  $\nabla_\perp \cdot \mathbf{z}_\perp^\pm = 0$ , the Alfvén speed is  $v_A = |\mathbf{B}_0|$ , and  $\mathbf{B}_0$  is in the  $z$  direction.

\* Contact e-mail: [alfred.mallet@unh.edu](mailto:alfred.mallet@unh.edu)

The turbulent system described by Eqs. (1) has several interesting characteristics. First, it is anisotropic with respect to the direction of the local magnetic field, as attested by numerical simulations (Shebalin et al. 1983; Oughton et al. 2004; Chen et al. 2011; Beresnyak 2015; Mallet et al. 2016) and solar-wind measurements (Horbury et al. 2008; Podesta 2009; Wicks et al. 2010; Chen et al. 2011; Chen 2016). This anisotropy can be understood in terms of the critical-balance conjecture (Goldreich & Sridhar 1995, 1997), whereby the linear (Alfvén) time  $\tau_A \sim l_\parallel/v_A$  ( $l_\parallel$  being the fluctuations’ coherence length along the magnetic field line) and nonlinear time  $\tau_{nl}$  should be similar to each other at all scales,  $\tau_A \sim \tau_{nl}$ .

Secondly, it has been noticed that at least in numerical simulations, there is a tendency for the different fields ( $\mathbf{z}_\perp^\pm, \mathbf{u}_\perp, \mathbf{b}_\perp$ ) to align with one another to within a small, scale-dependent angle  $\theta$  (Boldyrev 2006; Beresnyak & Lazarian 2006). In the nonlinear term in Eqs. (1), only  $\mathbf{z}_\perp^\pm$  with a gradient in the direction of  $\mathbf{z}_\perp^\mp$  gives rise to a nonzero contribution. Combined with the solenoidality of the RMHD fields, this implies that the alignment causes the nonlinearity to be noticeably suppressed. One can take this into account

by defining the nonlinear time as follows:

$$\tau_{\text{nl}}^{\pm} \doteq \frac{\lambda}{\delta z_{\perp}^{\pm} \sin \theta}. \quad (2)$$

If  $\sin \theta$  is scale-dependent, it may affect how the fluctuation amplitudes  $\delta z_{\perp}^{\pm}$  scale with the perpendicular scale  $\lambda$ . One can link the alignment effect to local anisotropy of the turbulent structures within the perpendicular plane. The aspect ratio of a sheet is related to the alignment angle between  $\delta \mathbf{u}_{\perp}$  and  $\delta \mathbf{b}_{\perp}$  fluctuations (see Boldyrev 2006) or between  $\delta z_{\perp}^{+}$  and  $\delta z_{\perp}^{-}$  fluctuations (see Chandran et al. 2015) via

$$\frac{\lambda}{\xi} \sim \sin \theta. \quad (3)$$

This 3D anisotropy has been measured in numerical simulations (Mallet et al. 2016; Verdini & Grappin 2015) and in the solar wind (Chen et al. 2012) (although in the latter case, it has not as yet been definitively pronounced scale-dependent).

The third key feature of Alfvénic turbulence, seen in both numerical simulations and in the solar wind, is its high degree of intermittency. Two related models of this intermittency that take into account critical balance and dynamic alignment (Mallet & Schekochihin 2017; Chandran et al. 2015, reviewed in Section 2) both show that, at each scale, higher-amplitude fluctuations are systematically more aligned and, therefore, more anisotropic in the perpendicular plane. Anticorrelation of alignment and amplitude has been confirmed in numerical simulations (Mallet et al. 2015, 2016).

Models of turbulence that incorporate dynamic alignment tend to predict perpendicular spectral indices close to  $-3/2$  (Boldyrev 2006; Chandran et al. 2015; Mallet & Schekochihin 2017), while the original "GS95" (Goldreich & Sridhar 1995) model, which does not include dynamic alignment, predicts a  $-5/3$  spectral index. Surprisingly, which of these two classes of models is correct has still not been settled numerically: while spectral indices measured in extremely high-resolution ( $2048^2 \times 512$ ) simulations are very close to  $-3/2$  (Perez et al. 2012, 2014), the scaling of the dissipation scale  $\lambda_{\eta}$  with Reynolds number ( $\text{Re} \doteq L_{\perp} \delta z / \eta$ , where  $\eta$  is the resistivity) in simulations with equivalent resolution appears to agree much better with the prediction using the GS95 model,  $\lambda_{\eta} \propto \text{Re}^{-3/4}$  (Beresnyak 2014). This suggests that there may be some small scale (perhaps relatively close to, but not smaller than, the dissipative scale predicted by the alignment theories) past which further alignment (or, equivalently, anisotropy within the perpendicular plane) breaks down.

In this paper, we propose a mechanism that causes the turbulent structures to stop aligning and becoming more sheetlike. It appears to be in the nature of the turbulence, at least at large scales, to dynamically generate coherent, large-amplitude, sheetlike structures. It is well known that sheetlike current structures are unstable to tearing modes<sup>1</sup> (Furth et al. 1963; Coppi et al. 1976), and that these modes can eventually disrupt initial sheetlike structures via magnetic reconnection (Loureiro et al. 2005; Uzdensky & Loureiro 2016; Tenerani et al. 2016). This paper attempts to answer the question of whether and at what scale this process occurs for the kind

of sheetlike structures that are dynamically formed by the aligning Alfvénic turbulence. It has recently been realized that, as current sheets form, they are violently unstable to the tearing instability, and so they never reach the idealized "Sweet-Parker" reconnection regime (Parker 1957; Sweet 1958; Loureiro et al. 2007; Pucci & Velli 2014; Tenerani et al. 2016; Uzdensky & Loureiro 2016) but instead break up into shorter sheets separated by magnetic islands. There are several stages in this process: the initial linear growth of the tearing instability, a possible Rutherford stage (Rutherford 1973) involving secular growth of the magnetic islands, and, finally, collapse of the X-points between the islands into short, Sweet-Parker-like sheets, which disrupt the initial structure by magnetic reconnection (Loureiro et al. 2005). The characteristic timescales of these processes, discussed in Section 3, make up the overall time needed to disrupt the sheet, which must be compared with the turbulent cascade time,  $\tau_{\text{C}} \sim \tau_{\text{nl}} \sim \tau_{\text{A}}$ , to determine if the disruption may occur. This is done in Section 4. We will determine the critical scale below which the sheetlike structures cannot survive, and also determine the number of magnetic islands that the sheets are broken into (see Sections 4.4 and 5). We will also discuss, in Section 6, the possible nature of the turbulence below the critical scale, and show that the disruption process (repeated in a recursive fashion) can potentially explain the controversy between the results of Perez et al. (2014) and Beresnyak (2014), as well as being an interesting physical example of turbulence creating the conditions needed for efficient dissipation of intense structures via rapid reconnection.

## 2 TURBULENCE PHENOMENOLOGY

The intermittency models of Chandran et al. (2015) (henceforth CSM15) and Mallet & Schekochihin (2017) (henceforth MS17) both envision structures that are characterized by amplitude  $\delta z$ , and characteristic scales  $l_{\parallel}$  (parallel scale),  $\lambda$  (perpendicular scale) and  $\xi$  (fluctuation-direction scale). Here we outline the scalings arising from these models that we will need in this work. Following Mallet & Schekochihin (2017), we introduce normalized variables

$$\delta \hat{z} = \frac{\delta z}{\overline{\delta z}}, \quad \hat{\lambda} = \frac{\lambda}{L_{\perp}}, \quad \hat{l}_{\parallel} = \frac{l_{\parallel}}{L_{\parallel}}, \quad \hat{\xi} = \frac{\xi}{L_{\perp}}, \quad (4)$$

where  $\overline{\delta z}$  is the outer-scale fluctuation amplitude, and  $L_{\perp}$  and  $L_{\parallel}$  are the perpendicular and parallel outer scales, respectively. The normalized amplitude in both models is given by  $\delta \hat{z} \sim \beta^q$ , where the non-negative random integer  $q$  is a Poisson random variable<sup>2</sup> with the mean  $\mu = -\ln \hat{\lambda}$ . The perpendicular scalings are, therefore, given in both models by

$$\langle \delta z^m \rangle \sim \hat{\lambda}^{\zeta_m^{\perp}} \quad (5)$$

with

$$\zeta_m^{\perp} = 1 - \beta^m, \quad (6)$$

where  $\beta$  is fixed via two different strategies in the two models: in MS17, the result is  $\beta = 1/\sqrt{2}$ , while in CSM15,  $\beta = 0.691$ . We will find it useful to define the "effective amplitude" of the structures that dominate the  $m$ -th order perpendicular structure function:

$$\langle \delta z^m | \hat{\lambda} \rangle \equiv (\delta \hat{z}[m])^m \sim \hat{\lambda}^{1-\beta^m}, \quad (7)$$

<sup>2</sup> Technically, in the MS17 model, the distribution of  $q$  conditional on  $\hat{\lambda}$  is a Poisson mixture, which, however, gives the same scalings for the structure functions as would be obtained with a pure Poisson-distributed  $q$ .

<sup>1</sup> One might also ask whether these sheets could be disrupted by the Kelvin-Helmholtz instability. However, since the vortex stretching terms for the different Elsasser fields have opposite sign (Zhdankin et al. 2016), in general, there will be more "current sheets" than "shear layers". In such sheets, the Kelvin-Helmholtz instability is suppressed (Chandrasekhar 1961).

and so

$$\delta\hat{z}[m] \sim \hat{\lambda}^{(1-\beta^m)/m}. \quad (8)$$

Note that  $(1-\beta^m)/m$  is a strictly decreasing function of  $m$ , and so  $m$  is a useful proxy for the amplitude of the structures at a given scale. Three cases in particular will be important. The first is  $m \rightarrow \infty$ , corresponding to the most intense structures with  $q = 0$ , which have amplitudes

$$\delta\hat{z}[\infty] \sim 1, \quad (9)$$

independent of  $\hat{\lambda}$ . Secondly, the "energy-containing" structures,  $m = 2$ , which determine the spectral index (since this is simply related to the scaling of the second-order structure function), and have amplitudes

$$\delta\hat{z}[2] \sim \hat{\lambda}^{1/4} \text{ (MS17)}, \quad \delta\hat{z}[2] \sim \hat{\lambda}^{0.26} \text{ (CSM15)}. \quad (10)$$

Finally, the limit  $m \rightarrow 0$  describes the "bulk" fluctuations with  $q = \mu$ , whose amplitudes are

$$\delta\hat{z}[0] \sim \hat{\lambda}^{-\ln\beta}. \quad (11)$$

In both models, the fluctuation-direction scale  $\hat{\xi}$  is given by

$$\hat{\xi} \sim \hat{\lambda}^\alpha \delta\hat{z}, \quad (12)$$

and the cascade time is

$$\tau_C \sim \tau_{nl} \sim \hat{\lambda}^{\kappa_1} \delta\hat{z}^{\kappa_2} \frac{L_\perp}{\delta z}. \quad (13)$$

In the MS17 model,

$$\alpha = \kappa_1 = 1/2, \quad \kappa_2 = 0, \quad (14)$$

while in the CSM15 model,

$$\alpha = 1 + \ln\beta, \quad \kappa_1 = (1 + \ln\beta)^2, \quad \kappa_2 = 1 + \ln\beta. \quad (15)$$

Both models envision structures that are sheetlike in the perpendicular plane, with length  $\xi$  and width  $\lambda$ , satisfying  $\xi \gg \lambda$ . Note that taking  $m = 2$  in the MS17 model recovers all the scalings of the original dynamic-alignment model due to Boldyrev (2006), but via a different derivation, and positing alignment between Elsasser fields, rather than between velocity and magnetic field. We will assume that the magnetic field varies by  $\delta B \sim \delta z$  across the sheet, and further assume that any velocity fluctuation  $\delta u \lesssim \delta B$  across the sheet<sup>3</sup> does not significantly alter the scalings of the tearing instability or its saturation. To determine whether and how structures of a particular amplitude are disrupted faster than they cascade, we must take a detailed look at the different timescales involved in the disruption process.

### 3 TIMESCALES

The process whereby a sheet of length  $\xi$  and width  $\lambda$ , with a magnetic field jump  $\delta B \sim \delta z$ , can be destroyed by reconnection occurs in several stages, which we will now briefly review, following Uzdensky & Loureiro (2016). First, there is exponential growth of the linear tearing mode until the width of the island(s) is approximately the width of the inner layer where resistivity is important,

$$w \sim \delta_{in} \sim [\gamma(k\delta z)^{-2}\lambda^2\eta]^{1/4}, \quad (16)$$

<sup>3</sup> The " $\lesssim$ " is important because for  $\delta u > \delta B$ , the Kelvin-Helmholtz mode dominates over the tearing mode. However, we neglect this situation for the reasons given in Footnote 1.

where  $\gamma$  is the linear growth rate of the tearing mode and  $k \sim N/\xi$  is its wavenumber ( $N$  is the number of islands). Secondly, there may be secular "Rutherford" growth of the islands until  $w \sim 1/\Delta'$ , where  $\Delta'$  is the instability parameter for the tearing mode. Thirdly, the X-point(s) that have arisen collapse into thin sheets, which then undergo fast reconnection, leaving behind a set of magnetic islands. We will examine these processes to determine which of them dominates the total time to disrupt the sheet, and thus determine whether this is faster than the cascade time  $\tau_C$ .

#### 3.1 Linear growth stage

We will assume that a typical sheetlike structure arising in dynamically aligning turbulence is reasonably well modelled by a Harris (1962) sheet, so

$$\Delta'\lambda = 2\left(\frac{1}{k\lambda} - k\lambda\right). \quad (17)$$

There is an instability provided that  $\Delta' > 0$ . We are interested in long-wavelength modes, so

$$\Delta'\lambda \sim \frac{1}{k\lambda} \sim \frac{\hat{\xi}}{N\hat{\lambda}}. \quad (18)$$

There are two possible situations: (i)  $\Delta'\delta_{in} \ll 1$ , "FKR" modes (Furth et al. 1963) with

$$\begin{aligned} \gamma_{\text{FKR}} &\sim \Delta'^{4/5} k^{2/5} \delta z^{2/5} \lambda^{-2/5} \eta^{3/5} \\ &\sim N^{-2/5} \left(\frac{\hat{\xi}}{\lambda}\right)^{2/5} S_\lambda^{-3/5} \frac{\delta z}{\lambda}, \end{aligned} \quad (19)$$

and (ii)  $\Delta'\delta_{in} \sim 1$ , "Coppi" modes (Coppi et al. 1976) with

$$\begin{aligned} \gamma_{\text{Coppi}} &\sim k^{2/3} \delta z^{2/3} \lambda^{-2/3} \eta^{1/3} \\ &\sim N^{2/3} \left(\frac{\hat{\xi}}{\lambda}\right)^{-2/3} S_\lambda^{-1/3} \frac{\delta z}{\lambda}, \end{aligned} \quad (20)$$

where the Lundquist number<sup>4</sup> is  $S_\lambda \doteq \lambda\delta z/\eta$ . Since these two modes have opposite dependence on  $k$ , the maximum growth rate can be found at the wavenumber where  $\gamma_{\text{FKR}} \sim \gamma_{\text{Coppi}}$ , giving

$$k_{\text{max}}\lambda \sim S_\lambda^{-1/4}, \quad \gamma_{\text{max}} \sim S_\lambda^{-1/2} \frac{\delta z}{\lambda}. \quad (21)$$

However, this "transitional mode" is only accessible if it actually fits into the sheet, i.e., if

$$k_{\text{max}}\xi \sim N_{\text{max}} \sim \frac{\hat{\xi}}{\lambda} S_\lambda^{-1/4} > 1. \quad (22)$$

The maximum growth rate for a particular structure is thus either  $\gamma_{\text{max}}$  given by Eq. (21), if  $k_{\text{max}}$  fits into the structure, or  $\gamma_{\text{FKR}}$  given by Eq. (19) with  $N = 1$ , the longest-wavelength FKR mode, otherwise.

#### 3.2 Rutherford growth stage

The linear growth stage ends when the width of the islands  $w \sim \delta_{in}$ , given by Eq. (16). If  $\Delta'w \ll 1$ , there will be secular "Rutherford" growth (Rutherford 1973) until  $\Delta'w \sim 1$ ,

$$w \sim \eta\Delta't. \quad (23)$$

<sup>4</sup> Note that  $S_\lambda$  is just what in turbulence theory one would usually call the local magnetic Reynolds number at scale  $\lambda$ .

If present, this stage lasts for a time

$$\tau_{\text{Ruth}} \sim \frac{1}{\eta \Delta^2} \sim N^2 \left( \frac{\hat{\lambda}}{\xi} \right)^2 S_{\perp} \frac{\lambda}{\delta z}. \quad (24)$$

Note that  $\tau_{\text{Ruth}}$  increases with  $N$ , so, if the maximum growth rate is attained for the  $N = 1$  FKR mode, this mode will also exit the Rutherford stage and saturate first. In the FKR limit,  $\Delta' \delta_{\text{in}} \ll 1$ , and so there is a well-defined Rutherford stage. For the Coppi modes,  $\Delta' \delta_{\text{in}} \sim 1$ , and so there is no Rutherford stage.

### 3.3 Collapse/reconnection stage

At the end of the Rutherford stage (or immediately after the linear stage in the case of Coppi modes), the  $X$ -point(s) formed by the tearing mode collapse into thin secondary sheets, each of length  $\sim \xi/N$ , and reconnect the flux in the original structure. This collapse, studied by Loureiro et al. (2005), results in exponential, Sweet-Parker-like growth of the reconnected flux on a timescale that, written in terms of our variables, is

$$\gamma_{\text{SP}} \sim S_{\perp}^{-1/2} \frac{\delta \hat{z}}{\lambda} \sim \gamma_{\text{max}}, \quad (25)$$

and so the rate of the collapse is always greater than or equal to the growth rate of the initial linear instability. Following Uzdensky & Loureiro (2016), we therefore do not need to consider the time associated with this stage in our determination of the disruption time of the original structure.

For high enough  $S_{L_{\perp}}$ , the collapse rate becomes independent of  $S_{\perp}$  because the Lundquist number associated with the secondary sheets becomes larger than  $S_c \sim 10^4$ , the critical Lundquist number required to trigger the onset of plasmoid-dominated fast reconnection (Loureiro et al. 2007; Samtaney et al. 2009; Bhattacharjee et al. 2009; Uzdensky et al. 2010; Loureiro et al. 2012). The critical  $S_{L_{\perp}}$  necessary to access the plasmoid-dominated regime will be determined in Section 4.5.

### 3.4 Disruption time

Based on the above scalings, we can now identify the disruption time as

$$\tau_{\text{D}} \sim \begin{cases} \max[1/\gamma_{\text{FKR}}, \tau_{\text{Ruth}}] & \text{if } \hat{\lambda} > \hat{\lambda}_{\text{tr}}, \\ 1/\gamma_{\text{max}} & \text{if } \hat{\lambda} \leq \hat{\lambda}_{\text{tr}}. \end{cases} \quad (26)$$

This is just restating the key result of Uzdensky & Loureiro (2016), which will allow us to compare  $\tau_{\text{D}}$  with the cascade time  $\tau_{\text{C}}$ . The transition scale  $\hat{\lambda}_{\text{tr}}$  will be worked out in Section 4.2.

### 3.5 Resistive time

If the structures are not able to be disrupted by reconnection, they can simply decay resistively on a timescale

$$\tau_{\eta} \sim \frac{\lambda^2}{\eta}. \quad (27)$$

The interesting question that we will answer in this paper is whether and under what circumstances this basic dissipation mechanism is superceded by tearing and the onset of reconnection.

## 4 CRITICAL SCALES

In this section, we will calculate the critical scales that partition the domain defined by  $\hat{\lambda}$  and  $m$  [see Eq. (8)] into regions where the structures are and are not disrupted by the onset of reconnection. To do this, we need to compare the timescales identified in section 3 to the cascade time  $\tau_{\text{C}}$  [Eq. (13)].

### 4.1 Resistive scale

First, we deal with the dissipative scale for the turbulence in the absence of any disruption by reconnection. Using Eqs. (13) and (27), we compare

$$\frac{\tau_{\text{C}}}{\tau_{\eta}} \sim \frac{\hat{\lambda}^{\kappa_1} \delta z^{\kappa_2} L_{\perp} \eta}{\lambda^2 \delta z} \sim \hat{\lambda}^{\kappa_1 - 2} \delta z^{\kappa_2} S_{L_{\perp}}^{-1}. \quad (28)$$

We consider fluctuations  $\delta \hat{z}[m]$  that are important for the  $m$ th-order structure function, using Eq. (8), to obtain

$$\frac{\tau_{\text{C}}}{\tau_{\eta}} \sim S_{L_{\perp}}^{-1} \hat{\lambda}^{\kappa_1 - 2 + \kappa_2 \zeta_m^{\perp}/m}. \quad (29)$$

Therefore, the resistive scale for these  $m$ th-order structures is

$$\hat{\lambda}_{\eta} \sim S_{L_{\perp}}^{-(2 - \kappa_1 - \kappa_2 \zeta_m^{\perp}/m)^{-1}}. \quad (30)$$

In the MS17 model, since  $\kappa_1 = 1/2$  and  $\kappa_2 = 0$ ,

$$\hat{\lambda}_{\eta}^{\text{MS}} \sim S_{L_{\perp}}^{-2/3}, \quad (31)$$

independent of  $m$ . This is the standard estimate for the dissipation scale (the analogue of the Kolmogorov scale) in the original dynamic-alignment model of Boldyrev (2006) (see, e.g., Perez et al. 2012 for an explicit derivation of this scaling). In the CSM15 model,

$$\hat{\lambda}_{\eta}^{\text{CSM}} \sim S_{L_{\perp}}^{-(1.60 - 0.63 \zeta_m^{\perp}/m)^{-1}}, \quad (32)$$

so the low-order, lower-amplitude fluctuations dissipate at smaller scales than the high-order, higher-amplitude fluctuations.

### 4.2 Boundary between FKR and transitional modes

The boundary between the two different regimes for the linear tearing stage is given by Eq. (22),  $S_{\perp}^{-1/4} \xi / \hat{\lambda} \sim 1$ . Using Eq. (12) and replacing  $\delta \hat{z}$  with the typical amplitude of an  $m$ th-order structure given by Eq. (8), we see that the transitional mode (21) may only occur when

$$\hat{\lambda} < \hat{\lambda}_{\text{tr}} \sim S_{L_{\perp}}^{\frac{1}{4} \left( \alpha - \frac{\alpha}{4} + \frac{3}{4} \frac{\zeta_m^{\perp}}{m} \right)^{-1}}. \quad (33)$$

In the MS17 model,

$$\hat{\lambda}_{\text{tr}}^{\text{MS}} \sim S_{L_{\perp}}^{-\frac{1}{3} (1 - \zeta_m^{\perp}/m)^{-1}}, \quad (34)$$

while in the CSM15 model,

$$\hat{\lambda}_{\text{tr}}^{\text{CSM}} \sim S_{L_{\perp}}^{\frac{1}{4} (-0.62 + 3 \zeta_m^{\perp}/4m)^{-1}}. \quad (35)$$

At scales  $\hat{\lambda} > \hat{\lambda}_{\text{tr}}$ , the FKR mode with  $N = 1$  is the most unstable linear mode, while at  $\hat{\lambda} < \hat{\lambda}_{\text{tr}}$ , the transitional mode (21) is the fastest.

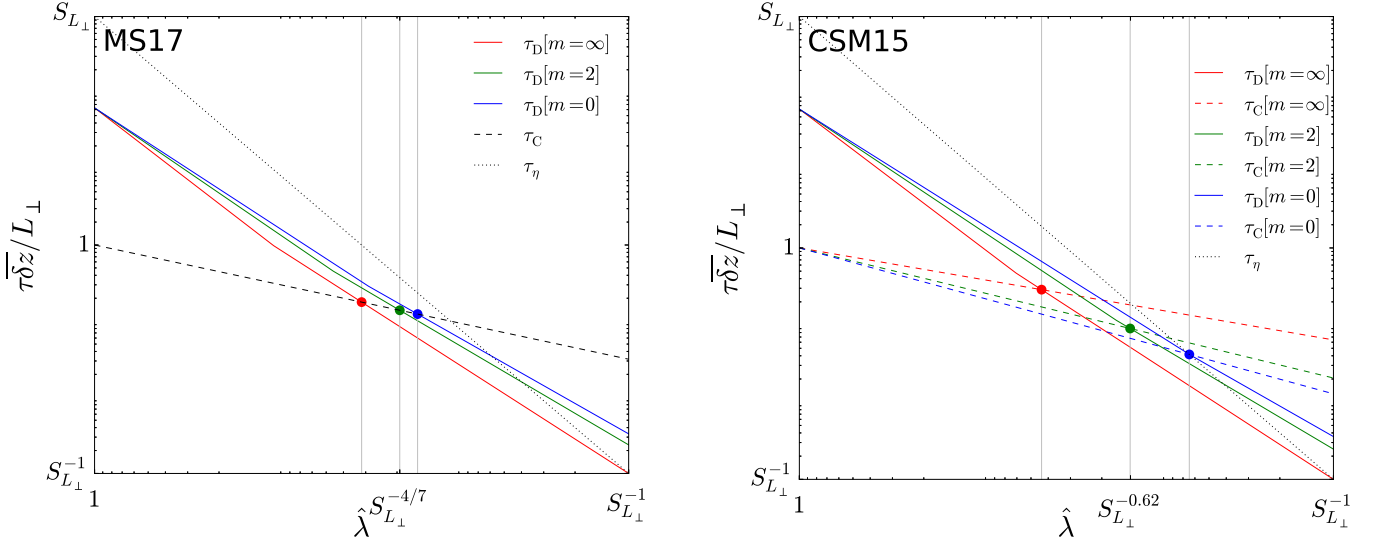


**Figure 1.** Comparison of the cascade timescale  $\tau_C$ , Eq. (13) (dashed lines), the disruption timescale  $\tau_D$ , Eq. (26) (solid, coloured lines) and the resistive timescale  $\tau_\eta$ , Eq. (27) (dotted lines), for the MS17 model (left panel) and the CSM15 panel (right panel). Where these timescales depend on the order  $m$  of the fluctuations, three values of  $m$  are plotted:  $m = \infty$  (in red),  $m = 2$  (in green) and  $m = 0$  (in blue). In the CSM15 model, not only  $\tau_D$  but also the cascade time varies with  $m$ , and so there are three curves for  $\tau_C$ . In the MS17 model,  $\tau_C$  does not depend on  $m$ , and so there is a single curve. The point at which the disruption process becomes faster than the turbulent cascade is marked with a circle for each  $m$ , and a gray vertical line marks the corresponding scale  $\hat{\lambda}_D[m]$ , given by Eqs. (44) for MS17 and (45) for CSM15.

### 4.3 Linear FKR critical scale

To determine whether the  $N = 1$  FKR mode grows fast enough to disrupt the structures, we first calculate, using Eqs. (19), (12), (13) and (8),

$$\begin{aligned} \gamma_{\text{FKR}}[N = 1]\tau_C &\sim \left(\frac{\hat{\xi}}{\hat{\lambda}}\right)^{2/5} S_{L_\perp}^{-3/5} \frac{\delta\hat{z}}{\hat{\lambda}} \hat{\lambda}^{\kappa_1} \delta\hat{z}^{\kappa_2} \\ &\sim S_{L_\perp}^{-3/5} \hat{\lambda}^{\frac{2\alpha}{5} - 2 + \kappa_1} \delta\hat{z}^{\frac{4}{5} + \kappa_2} \\ &\sim S_{L_\perp}^{-3/5} \hat{\lambda}^{\frac{2\alpha}{5} - 2 + \kappa_1 + \frac{\zeta_m^\perp}{m} (\frac{4}{5} + \kappa_2)}. \end{aligned} \quad (36)$$

The sheet will not be disrupted unless  $\gamma_{\text{FKR}}[N = 1]\tau_C > 1$ . This is equivalent to

$$\hat{\lambda} < \hat{\lambda}_{\text{FKR}} \sim S_{L_\perp}^{\frac{3}{5} \left[ \frac{2\alpha}{5} - 2 + \kappa_1 + \frac{\zeta_m^\perp}{m} (\frac{4}{5} + \kappa_2) \right]^{-1}}. \quad (37)$$

For the MS17 model,

$$\hat{\lambda}_{\text{FKR}}^{\text{MS}} \sim S_{L_\perp}^{-\frac{6}{13} \left( 1 - \frac{8\zeta_m^\perp}{13m} \right)^{-1}}, \quad (38)$$

while for the CSM15 model,

$$\hat{\lambda}_{\text{FKR}}^{\text{CSM}} \sim S_{L_\perp}^{-\frac{3}{5} \left( 1.35 - \frac{1.43\zeta_m^\perp}{m} \right)^{-1}}. \quad (39)$$

Comparing these scalings with Eq. (33), we see that the scale  $\hat{\lambda}_{\text{FKR}}$  is smaller than the corresponding  $\hat{\lambda}_{\text{tr}}$  for all  $m$ , and so there are no FKR modes that grow fast enough to disrupt the structures. Therefore, we do not need to consider the duration of the Rutherford stage (see Section 3.2) to determine whether disruption occurs.

### 4.4 Disruption scale

For a given  $m$ , at  $\hat{\lambda} \leq \hat{\lambda}_{\text{tr}}$ , with the latter scale given by Eq. (33), the disruption time is, therefore,

$$\tau_D \sim 1/\gamma_{\text{max}}, \quad (40)$$

and we must calculate

$$\begin{aligned} \gamma_{\text{max}}\tau_C &\sim S_{L_\perp}^{-1/2} \frac{\delta\hat{z}}{\hat{\lambda}} \hat{\lambda}^{\kappa_1} \delta\hat{z}^{\kappa_2} \\ &\sim \hat{\lambda}^{-3/2 + \kappa_1 + (1/2 + \kappa_2)\zeta_m^\perp/m} S_{L_\perp}^{-1/2}, \end{aligned} \quad (41)$$

where we have used Eq. (21) for  $\gamma_{\text{max}}$  and Eqs. (13) and (8) to express  $\tau_C$  and  $\delta\hat{z}$  in terms of  $\hat{\lambda}$  and  $m$ . The sheet will be disrupted if  $\gamma_{\text{max}}\tau_C > 1$ . This happens for

$$\hat{\lambda} < \hat{\lambda}_D \sim S_{L_\perp}^{-\frac{1}{2} \left[ \frac{3}{2} - \kappa_1 - (\frac{1}{2} + \kappa_2) \frac{\zeta_m^\perp}{m} \right]^{-1}}. \quad (42)$$

The corresponding number of islands, from Eq. (22), is

$$\begin{aligned} N_D &\sim S_{L_\perp}^{-1/4} \frac{\hat{\xi}_D}{\hat{\lambda}_D} \\ &\sim \hat{\lambda}_D^{\alpha - 5/4 + 3\zeta_m^\perp/4m} S_{L_\perp}^{-1/4}, \\ &\sim S_{L_\perp}^{\frac{1}{2} \left\{ \left( \frac{3}{2} - \alpha - \frac{3\zeta_m^\perp}{4m} \right) \left[ \frac{3}{2} - \kappa_1 - (\frac{1}{2} + \kappa_2) \frac{\zeta_m^\perp}{m} \right]^{-1} - \frac{1}{4} \right\}}. \end{aligned} \quad (43)$$

In the MS17 model, these scalings become

$$\hat{\lambda}_D^{\text{MS}} \sim S_{L_\perp}^{-\frac{1}{2} \left( 1 - \frac{\zeta_m^\perp}{2m} \right)^{-1}}, \quad N_D^{\text{MS}} \sim S_{L_\perp}^{\frac{1 - 2\zeta_m^\perp/m}{8 - 4\zeta_m^\perp/m}}, \quad (44)$$

while in the CSM15 model,

$$\hat{\lambda}_D^{\text{CSM}} \sim S_{L_\perp}^{-0.45 \left( 1 - 1.03\zeta_m^\perp/m \right)^{-1}}, \quad N_D^{\text{CSM}} \sim S_{L_\perp}^{-\frac{1}{4} + \frac{0.309 - 3\zeta_m^\perp/8m}{1.10 - 1.13\zeta_m^\perp/m}}. \quad (45)$$

These scalings determine the largest  $\hat{\lambda}$  for which the fastest-growing mode reaches collapse in a time shorter than the cascade

time  $\tau_C$  of the turbulence, and, therefore, the smallest  $\hat{\lambda}$  for which the aligned, sheetlike structures can survive. We will examine some instructive particular cases and the physical consequences of these results in Sections 5 and 6.

#### 4.5 Critical $S_{L_\perp}$ for the plasmoid-dominated regime

As an interesting aside, we noted in Section 3.3 that for high enough  $S_{L_\perp}$ , the reconnection rate  $\gamma_{SP}$  becomes independent of  $S_\lambda$  due to the onset of the plasmoid instability. For this to occur, the Lundquist number associated with the secondary sheets must be

$$S_{\hat{\lambda}_D/N_D} \sim \hat{\lambda}_D \delta \hat{z}_{\hat{\lambda}_D} S_{\hat{\lambda}_D}^{1/4} S_{L_\perp} \sim \hat{\lambda}_D^{\frac{5}{4}(1+\epsilon_m^{\perp}/m)} S_{L_\perp}^{5/4} > S_c, \quad (46)$$

where we used Eq. (22) for  $N_D = N_{\max}$ . Expressing this condition in terms of  $S_{L_\perp}$ , we obtain in the MS17 model, using Eq. (44),

$$S_{L_\perp} > S_c^{\frac{4}{5} \frac{1-\epsilon_m^{\perp}/2m}{1/2-\epsilon_m^{\perp}/m}}. \quad (47)$$

For such values of  $S_{L_\perp}$ , the secondary sheets will break into plasmoids and the reconnection/collapse rate will be given by

$$\gamma_{\text{plasmoids}} \sim S_c^{-1/2} \frac{\delta \hat{z}}{\hat{\lambda}}, \quad (48)$$

instead of Eq. (25), because the secondary sheet will be broken into "critical Sweet-Parker sheets" (Uzdensky et al. 2010), each of which will reconnect at this rate. Assuming  $S_c \sim 10^4$  (Loureiro et al. 2007; Samtaney et al. 2009),<sup>5</sup> the critical  $S_{L_\perp}$  given by Eq. (47) is quite high: for the  $m = \infty$  structures to be plasmoid unstable,  $S_{L_\perp} \gtrsim S_c^{8/5} \sim 10^6$ , while for the  $m = 2$  structures,  $S_{L_\perp} \gtrsim S_c^{14/5} \sim 10^{11}$ . The critical  $S_{L_\perp}$  is much higher than the critical Lundquist number for a Sweet-Parker sheet to be plasmoid unstable because the structures formed by the turbulence do not have a particularly high aspect ratio. The mechanism outlined in this paper does not rely on the secondary sheets being plasmoid unstable: for the disruption to occur, we only need  $\tau_C/\tau_D > 1$ , where  $\tau_D$  is set by the tearing growth rate.

### 5 TRANSITION TO A NEW REGIME OF STRONG ALFVÉNIC TURBULENCE

The comparison of timescales in Section 4 has allowed us to predict the scale at which the sheetlike structures at each order  $m$  are disrupted by the onset of reconnection. While the cascade time  $\tau_C$  [Eq. (13)] decreases as the cascade progresses to smaller scales, so does the disruption time  $\tau_D$  [Eq. (26)], due to the increasing aspect ratio of the aligned sheetlike structures. This is shown in Figure 1 for both the MS17 and CSM15 models, for  $m = \infty, 2, 0$  (most intense, energy-containing, and most typical structures, respectively). Also shown are the disruption scales  $\hat{\lambda}_D[m]$  beyond which the sheetlike structures of order  $m$  cannot survive.

The effect that the disruption has on the turbulence is, thus, as follows: for  $\hat{\lambda} < \hat{\lambda}_D$ , the sheetlike structures predicted by the turbulence models that rely on dynamic alignment (e.g., MS17, CSM15, and the original model of Boldyrev 2006) are disrupted by reconnection into several separate islands. The detailed dependence of  $\hat{\lambda}_D$

on  $m$  in the MS17 and CSM15 models [Eqs. (44) and (45), respectively] is shown in Figure 2, along with the resistive scales corresponding to these models [Eqs. (31) and (32)]. The disruption scale  $\hat{\lambda}_D$  is an increasing function of  $m$ , and as  $m \rightarrow \infty$  it approaches

$$\hat{\lambda}_D^{\text{MS}}[\infty] \sim S_{L_\perp}^{-1/2}, \quad \hat{\lambda}_D^{\text{CSM}}[\infty] \sim S_{L_\perp}^{-0.45}, \quad (49)$$

in the MS17 and CSM15 models, respectively. One might expect to see a change in the spectral index (since this is related to the scaling exponent of the second-order structure function) at around

$$\hat{\lambda}_D^{\text{MS}}[2] \sim S_{L_\perp}^{-4/7}, \quad \hat{\lambda}_D^{\text{CSM}}[2] \sim S_{L_\perp}^{-0.62}. \quad (50)$$

Dynamically, the transition could probably be considered complete at  $\hat{\lambda}_D[2]$ , because all structures with energetically significant amplitudes have been disrupted, but we can also calculate the point at which the transition is complete even for very low-amplitude fluctuations: for  $m = 0$  structures, the disruption scale is given by

$$\hat{\lambda}_D^{\text{MS}}[0] \sim S_{L_\perp}^{-0.60}, \quad \hat{\lambda}_D^{\text{CSM}}[0] \sim S_{L_\perp}^{0.73}. \quad (51)$$

Note that for all  $m$ , the disruption scale is above the resistive scale,  $\hat{\lambda}_D > \hat{\lambda}_\eta$  (see Section 4.1). Roughly speaking, one might expect the behaviour of the  $m$ th-order structure function to change at  $\hat{\lambda}_D[m]$ . In practice, since structures of all orders contribute to all structure functions to differing degrees, the transition will take place over a range of scales between  $\hat{\lambda}_D[\infty]$  and  $\hat{\lambda}_D[0]$ .

### 6 TURBULENCE BELOW $\hat{\lambda}_D$

It is natural to ask what happens to the turbulence below the disruption scale  $\hat{\lambda}_D$ . First, we expect the sheetlike structures just above  $\hat{\lambda}_D$  to be broken up into "flux-rope-like" structures just below  $\hat{\lambda}_D$ : circular in the perpendicular plane, with scale  $\hat{\lambda}_D$ ,<sup>6</sup> but extended in the direction parallel to the local magnetic field, due to critical balance. Secondly, we also expect some fraction of the energy to be dissipated via the reconnection process. Thirdly, we expect these structures to behave as they normally would in Alfvénic turbulence: to interact, dynamically align, and cascade to smaller scales. The only change compared to the "primary cascade" is that the disruption process effectively resets the perpendicular anisotropy at scale  $\hat{\lambda}_D$ , and potentially dissipates some fraction  $1 - A^2$  of the structures' energy, so the aligning structures have smaller aspect ratios than they would have done without the disruption. They will eventually, in turn, be disrupted at a secondary disruption scale, and so on. Therefore, what we have so far called  $\hat{\lambda}_D$  is only the first of many subsequent disruption scales – and so from now on, we will call this first disruption scale  $\hat{\lambda}_{D,1}$ . We can therefore identify two distinct subranges:

$\hat{\lambda} > \hat{\lambda}_{D,1}$ , "free alignment range",

$\hat{\lambda} < \hat{\lambda}_{D,1}$ , "disruption range".

The two subranges are shown in Figure 2, along with our prediction for the final dissipation scale  $\hat{\lambda}_{\eta,\infty}$ , discussed in Section 6.2. We now proceed to discuss the sequence of disruptions, and then the eventual dissipation scale for the turbulence. We will restrict ourselves to the case of  $m = 2$  for the following discussion, i.e., we omit any discussion of the intermittency in the disruption range.

<sup>5</sup> Note that in a turbulent environment,  $S_c$  may be somewhat lower, possibly by as much as an order of magnitude (see Loureiro et al. 2009).

<sup>6</sup> Based on the numerical evidence in Loureiro et al. (2005), this does appear to be how the tearing mode saturates at high enough  $\Delta$ .

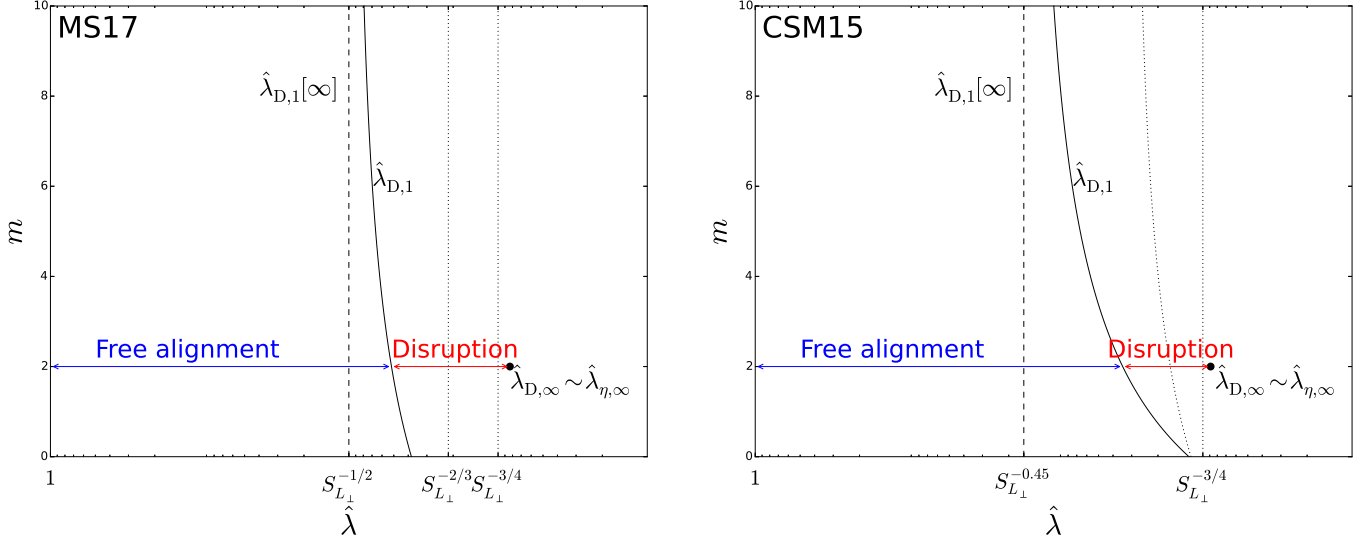


**Figure 2.** The solid black line shows the dependence of  $\hat{\lambda}_{D,1}$  on  $m$  in the MS17 model [Eq. (44), left panel] and in the CSM15 model [Eq. (45), right panel]. The dashed lines show  $\hat{\lambda}_{D,1}[m = \infty]$ . The two different subranges for the  $m = 2$  structures are marked by blue and red arrows. The leftmost (i.e., larger scale) dotted line on each plot shows the expected dissipation scales (31) and (32) of the Alfvénic turbulence without disruption, while the rightmost (smaller scale) dotted line shows the Kolmogorov scale,  $S_{L_\perp}^{-3/4}$  [Eq. (65)]. The black point shows the value of the final dissipation scale of the disrupted turbulence  $\hat{\lambda}_{D,\infty} \sim \hat{\lambda}_{\eta,\infty}$  [Eq. (56)]. We have set  $A^2 = 0.5$  and  $S_{L_\perp} = 10^4$  in this figure.

### 6.1 Recursive disruption

The series of subsequent disruptions can be understood as follows. After the  $(P - 1)$ st disruption, the turbulence behaves as though there is a  $P$ th cascade, with "outer-scale" values of the turbulent variables given by the values at the  $(P - 1)$ st disruption scale,  $\hat{\lambda}_{D,P-1}$ . The cascade has the same scalings as the original cascade, but with the replacements

$$L_\perp \rightarrow \lambda_{D,P-1}, \quad \overline{\delta z} \rightarrow A \overline{\delta z} \hat{\lambda}_{D,P-1}^{\zeta_2^\perp/2}, \quad (52)$$

in all places where either of these variables appear (including normalizations). The constant  $A$  encodes the fact that we expect some fixed fraction  $1 - A^2$  of the disrupted structure's energy to be dissipated via the reconnection process<sup>7</sup>. Using the rule (52) in Eqs. (44), (45) for  $\hat{\lambda}_D$  leads to the recursive relation

$$\hat{\lambda}_{D,P} \sim \hat{\lambda}_{D,P-1}^{1+f_D(1+\zeta_2^\perp/2)} (AS_{L_\perp})^{f_D}, \quad (53)$$

This scale has been normalized the scales by  $L_\perp$  after performing the replacement procedure (52). The exponent  $f_D$  depends on the choice of turbulence model, and is the exponent in Eqs. (44) or (45) for each model, with  $m = 2$ ,

$$f_D = \begin{cases} -\frac{1}{2} \left(1 - \frac{\zeta_2^\perp}{4}\right)^{-1}, & \text{MS17 \& B06 models,} \\ -0.45 \left(1 - 0.52\zeta_2^\perp\right)^{-1}, & \text{CSM15 model,} \end{cases} \quad (54)$$

where we have denoted the **Boldyrev (2006)** model as B06 (it has the same scalings at  $m = 2$  as MS17). The recursion relation (53)

<sup>7</sup> This does not imply that there are sharp jumps in the structure function. As the cascade progresses to smaller scales, the fraction of the energy contained in disrupted structures increases continuously: the disruption scale is just the scale at which a given structure function is dominated by disrupted structures.

may be written as

$$\hat{\lambda}_{D,P} \sim \hat{\lambda}_{D,1}^{[1+f_D(1+\zeta_2^\perp/2)]^{P-1}} (AS_{L_\perp})^{f_D \sum_{p=0}^{P-2} [1+f_D(1+\zeta_2^\perp/2)]^p}. \quad (55)$$

As  $P \rightarrow \infty$ , we have

$$\hat{\lambda}_{D,\infty} \sim (AS_{L_\perp})^{(1+\zeta_2^\perp/2)^{-1}}. \quad (56)$$

Figure 3 shows the scale  $\hat{\lambda}_{D,P}$ , for  $P = 1, 2, 3, \dots, \infty$ , in both the MS17 and CSM15 models. One can see that as  $P$  increases, the successive disruptions become ever closer to each other in scale, with the disruption scale tending to the asymptotic value (56), given in the MS17 model by

$$\hat{\lambda}_{D,\infty} \sim (AS_{L_\perp})^{-4/5}, \quad (57)$$

and in the CSM15 model by

$$\hat{\lambda}_{D,\infty} \sim (AS_{L_\perp})^{-0.79}. \quad (58)$$

### 6.2 Final dissipative cutoff scale

Similarly to Eq. (53), using the rule (52) in Eqs. (31), (32) for  $\hat{\lambda}_\eta$  leads to the recursive relation

$$\hat{\lambda}_{\eta,P} \sim \hat{\lambda}_{\eta,P-1}^{1+f_\eta(1+\zeta_2^\perp/2)} (AS_{L_\perp})^{f_\eta}, \quad (59)$$

where the exponent  $f_\eta$  is given by the exponents of Eqs. (31) or (32):

$$f_\eta = \begin{cases} -2/3, & \text{MS17 \& B06 models,} \\ -(1.60 - 0.32\zeta_2^\perp)^{-1}, & \text{CSM15 model.} \end{cases} \quad (60)$$

The limit of  $\hat{\lambda}_{\eta,P}$  as  $P \rightarrow \infty$  is also given by (56), so

$$\hat{\lambda}_{\eta,\infty} \sim \hat{\lambda}_{D,\infty} \sim (AS_{L_\perp})^{(1+\zeta_2^\perp/2)^{-1}}. \quad (61)$$

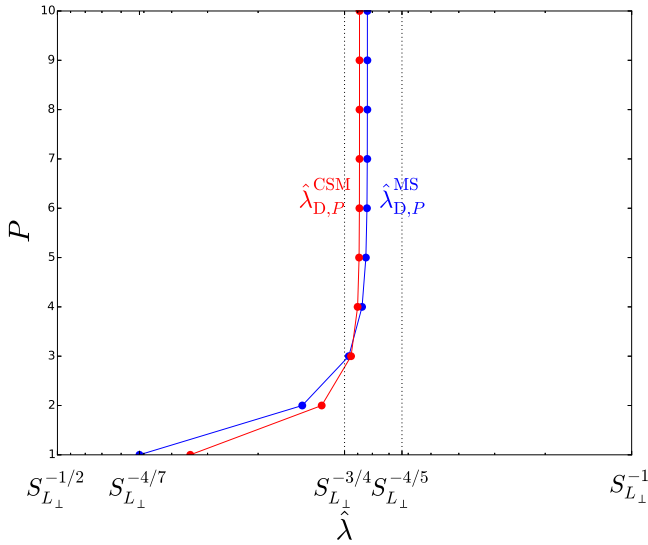


**Figure 3.** The dependence of  $\hat{\lambda}_{D,P}$  on  $P$  [Eq. (55)] is shown for the MS17 model (blue) and the CSM15 model (red). The Kolmogorov scale given by Eq. (65), and the scale  $S_{L_\perp}^{-4/5}$  [the scale  $\hat{\lambda}_{\eta,\infty}$  if  $A = 1$ , given by Eq. (62)] are shown as black dotted lines for comparison. We have set  $A^2 = 0.5$  and  $S_{L_\perp} = 10^4$  in this figure.

Since  $f_D > f_\eta$  for both models,  $\hat{\lambda}_{D,P} > \hat{\lambda}_{\eta,P}$  for all  $P < \infty$ , and  $\hat{\lambda}_{\eta,\infty}$  may be considered the final dissipation scale for the cascade. In the MS17 model, we obtain

$$\hat{\lambda}_{\eta,\infty} \sim (AS_{L_\perp})^{-4/5}, \quad (62)$$

and in the CSM15 model,

$$\hat{\lambda}_{\eta,\infty} \sim (AS_{L_\perp})^{-0.79}. \quad (63)$$

These scalings are nearly identical, since the scaling exponents  $\zeta_2^\perp$  are extremely close in the two models.

A rescaling of the energy spectrum by the final dissipation scale  $\hat{\lambda}_{\eta,\infty}$  should be performed to compare our results with numerical simulations (see Beresnyak 2014 for a detailed discussion of how to perform such a rescaling). The apparent scaling of the dissipation scale with  $S_{L_\perp}$  also depends on the constant  $A$ . For a system with Reynolds/Lundquist number  $S_{L_\perp}$ , the dissipation scale (61) may be written

$$\hat{\lambda}_{\eta,\infty} \sim S_{L_\perp}^{-(1+c)(1+\zeta_2^\perp/2)^{-1}}, \quad (64)$$

where  $c = \ln A / \ln S_{L_\perp}$ . Assuming that the reconnection is relatively efficient, say  $A^2 \approx 0.5$  (Loureiro et al. 2012), one finds that for currently numerically accessible values of  $S_{L_\perp} \approx 10^4$ , the effective scaling is close to the Kolmogorov scaling

$$\hat{\lambda}_\eta^{K41} \sim S_{L_\perp}^{-3/4}, \quad (65)$$

expected for a turbulent cascade with a  $-5/3$  spectral index, consistent with the conclusions of Beresnyak (2014). The Kolmogorov scale  $S_{L_\perp}^{-3/4}$  is plotted as a vertical dotted line in Figures 2 and 3, and it is clearly rather close to  $\hat{\lambda}_{\eta,\infty}$  in both models. In the limit of  $S_{L_\perp} \rightarrow \infty$ ,  $c \rightarrow 0$ , but this convergence is logarithmically slow. Therefore, the Kolmogorov scaling may be practically indistinguishable from the  $S_{L_\perp}^{-0.8}$  scaling [Eqs. (62) and (63)] of the final dissipation scale.

If, instead of rescaling the energy spectrum by  $\hat{\lambda}_{\eta,\infty}$ , one looks

for some "effective dissipation scale" at which the spectrum stops behaving like an approximately  $k^{-3/2}$  power law, one will obtain a different result: because of the dissipation at each disruption, the amplitude will drop significantly compared to the  $k^{-3/2}$  scaling before  $\hat{\lambda}_{\eta,\infty}$ , and the spectrum in the range  $\hat{\lambda}_{D,1}^{-1} \sim S_{L_\perp}^{4/7} < k < \hat{\lambda}_{\eta,\infty}^{-1}$  will be steeper than the approximately  $k^{-3/2}$  scaling of the underlying  $m = 2$  fluctuations. It is tempting to conjecture that the "effective spectral index" in this range may be close to the  $-5/3$  of the Goldreich & Sridhar (1995) model, but because we do not have an analytical model for the spectrum in the disruption range, we have instead concentrated on the scaling of the dissipative cutoff.

Thus, the change in the character of the turbulence due to the disruption by reconnection might explain the recent controversy over the measured scalings of the RMHD spectrum in very high-resolution numerical simulations, where, despite measuring very clean  $k_\perp^{-3/2}$  spectra in the inertial range (e.g., Perez et al. 2014), as predicted by the theories involving dynamic alignment (Boldyrev 2006; Chandran et al. 2015; Mallet & Schekochihin 2017), the dependence of the dissipation scale on viscosity or resistivity<sup>8</sup> (Beresnyak 2014) agrees much better with the Kolmogorov scaling (65). Effectively, both sets of measurements are correct, but neither tells the "full story": at large scales, dynamic alignment occurs, but at sufficiently small scales, the sheetlike structures become unstable, which limits the alignment, steepens the spectrum and forces the dissipation scale to have different scaling properties, which, as we have shown, may be close to the Kolmogorov scaling for currently feasible simulations.

It is perhaps worth commenting on how one might expect the scaling of the traditional alignment angles based on ratios of structure functions involving angles between different RMHD fields (Mason et al. 2006; Beresnyak & Lazarian 2006) to change in the disruption range. Because there is a physical lower limit to the alignment angle of turbulent structures in this range, these alignment measures might possibly have a shallower scaling exponent at scales below  $\hat{\lambda}_{D,1}$ , despite the fact that all the structures are still dynamically aligning between successive disruptions as they cascade. Shallower scaling exponents for these measures were in fact observed at the smallest scales in the numerical simulations of both Perez et al. (2012, 2014) and Beresnyak (2012).

## 7 DISCUSSION

The dynamic-alignment models of strong Alfvénic turbulence due to Boldyrev (2006), Chandran et al. (2015) and Mallet & Schekochihin (2017) all predict that, as turbulent structures cascade to smaller scales, the vector fluctuations within them progressively align, and the structures become progressively more sheetlike and anisotropic within the perpendicular plane. In this paper, inspired by the recent work on the disruption of forming current sheets by Uzdensky & Loureiro (2016), we have found that these sheetlike structures are destroyed by reconnection below a certain scale  $\hat{\lambda}_D$ . This disruption process occurs in two stages: linear growth of a tearing instability with multiple islands, and then collapse of the  $X$ -points between these islands into thin current sheets, which reconnect until the original structure has been destroyed. This means that the linear growth rate must be large compared to the cascade rate of the turbulence in order for the structures to be

<sup>8</sup> The simulations were done with equal viscosity and resistivity.

disrupted. To estimate the timescales involved, we have used scalings from the turbulence models of Mallet & Schekochihin (2017) and Chandran et al. (2015). Qualitatively, these models give similar results, although quantitatively the predicted scalings are slightly different.

We find that there is a critical scale  $\hat{\lambda}_D \sim S_{L_1}^{-0.6}$  below which the turbulent structures are disrupted. This means that the turbulence theories that rely on dynamic alignment can only be expected to give accurate predictions at scales above  $\hat{\lambda}_D$ . At  $\hat{\lambda}_D$ , the turbulent cascade is effectively reset to unaligned structures, which can now cascade to smaller scales and again become progressively more sheetlike and aligned. We show that they are recursively disrupted at a sequence of smaller scales  $\hat{\lambda}_{D,P}$ , with  $P = 2, \dots, \infty$ , until they reach a final dissipation scale  $\hat{\lambda}_{\eta,\infty} \sim S_{L_1}^{-0.8}$ . This is a smaller scale than the dissipation scale predicted by the dynamic-alignment theories (Boldyrev 2006; Chandran et al. 2015; Mallet & Schekochihin 2017), and is close to the Kolmogorov scaling  $\hat{\lambda}_\eta \sim S_{L_1}^{-0.75}$  for currently feasible numerical simulations. This is despite the fact that the spectral index above  $\hat{\lambda}_D$  in our model is approximately  $-3/2$  typical of the dynamic-alignment theories. Thus, our argument that sheetlike structures are disrupted by reconnection below  $\hat{\lambda}_D$  might explain the discrepancy between the measured  $-3/2$  spectrum in numerical simulations (Perez et al. 2014), and the seemingly opposing evidence that the dissipation range is much better described by the Goldreich-Sridhar/Kolmogorov scaling for the dissipation scale (Beresnyak 2014).

There are many improvements possible to the simple model of the disruption process that we have outlined here. First, we have neglected the effects of shear and viscosity on the stability of current layers (Chen & Morrison 1990a,b). Secondly, our conjectures about the turbulence below  $\hat{\lambda}_D$  are rather simple: we completely ignore the intermittency in this range, and do not take into account anything about the specific nature of the island structures produced by the tearing instabilities, apart from the fact that there is a limit on their anisotropy in the perpendicular plane. Thirdly, in many situations (including the solar wind), kinetic scales will intervene at some point in the collapse process, significantly altering the dynamics. Nevertheless, we expect the idea that the sheetlike structures produced by dynamically aligning turbulence will eventually reconnect and destroy themselves is robust, even in kinetic systems, and provides an interesting link between inertial-range intermittent turbulent structures and efficient dissipation via magnetic reconnection.

## ACKNOWLEDGEMENTS

We thank A. Beresnyak and N. Loureiro for useful conversations. While this manuscript was in an advanced stage of preparation, we became aware that a similar calculation of the disruption scale of sheetlike structures in Alfvénic turbulence was concurrently being done by N. Loureiro and S. Boldyrev. We are grateful to N. Loureiro for alerting us to this work. The work of A.M. was supported by the NASA grant NNX15AI80G and NSF grant PHY-1500041. The work of A.A.S. was supported in part by grants from UK STFC and EPSRC. A.M. and A.A.S. would like to acknowledge the hospitality of the Wolfgang Pauli Institute, Vienna, where the idea behind this work was first conceived.

## REFERENCES

Beresnyak A., 2012, *MNRAS*, **422**, 3495

*MNRAS* **000**, 1–?? (2016)

- Beresnyak A., 2014, *ApJ*, **784**, L20  
 Beresnyak A., 2015, *ApJ*, **801**, L9  
 Beresnyak A., Lazarian A., 2006, *ApJ*, **640**, L175  
 Bhattacharjee A., Huang Y.-M., Yang H., Rogers B., 2009, *Phys. Plasmas*, **16**, 112102  
 Boldyrev S., 2006, *Phys. Rev. Lett.*, **96**, 115002  
 Bruno R., Carbone V., 2013, *Living Rev. Solar Phys.*, **10**, 2  
 Chandran B. D. G., Schekochihin A. A., Mallet A., 2015, *ApJ*, **807**, 39  
 Chandrasekhar S., 1961, *Hydrodynamic and Hydromagnetic Stability*. Oxford University Press  
 Chen C. H. K., 2016, *J. Plasma Phys.*, **82**(6)  
 Chen X., Morrison P., 1990a, *Phys. Fluids B*, **2**, 495  
 Chen X., Morrison P., 1990b, *Phys. Fluids B*, **2**, 2575  
 Chen C. H. K., Mallet A., Yousef T. A., Schekochihin A. A., Horbury T. S., 2011, *MNRAS*, **415**, 3219  
 Chen C. H. K., Mallet A., Schekochihin A. A., Horbury T. S., Wicks R. T., Bale S. D., 2012, *ApJ*, **758**, 120  
 Coppi B., Pellat R., Rosenbluth M., Rutherford P., Galvao R., 1976, *Sov. J. Plasma Phys.*, **2**  
 Elsasser W. M., 1950, *Phys. Rev.*, **79**, 183  
 Furth H. P., Killeen J., Rosenbluth M. N., 1963, *Phys. Fluids*, **6**, 459  
 Goldreich P., Sridhar S., 1995, *ApJ*, **438**, 763  
 Goldreich P., Sridhar S., 1997, *ApJ*, **485**, 680  
 Harris E. G., 1962, *Nuovo Cimento*, **23**, 115  
 Horbury T. S., Forman M., Oughton S., 2008, *Phys. Rev. Lett.*, **101**, 175005  
 Loureiro N. F., Cowley S. C., Dorland W. D., Haines M. G., Schekochihin A. A., 2005, *Phys. Rev. Lett.*, **95**, 235003  
 Loureiro N. F., Schekochihin A. A., Cowley S. C., 2007, *Phys. Plasmas*, **14**, 100703  
 Loureiro N. F., Uzdensky D. A., Schekochihin A. A., Cowley S. C., Yousef T. A., 2009, *MNRAS*, **399**, L146  
 Loureiro N. F., Samtaney R., Schekochihin A. A., Uzdensky D. A., 2012, *Phys. Plasmas*, **19**, 042303  
 Mallet A., Schekochihin A. A., 2017, in press, *MNRAS*, arXiv:1606.00466  
 Mallet A., Schekochihin A. A., Chandran B. D. G., 2015, *MNRAS*, **449**, L77  
 Mallet A., Schekochihin A. A., Chandran B. D. G., Chen C. H. K., Horbury T. S., Wicks R. T., Greenan C. C., 2016, *MNRAS*, **459**, 2130  
 Mason J., Cattaneo F., Boldyrev S., 2006, *Phys. Rev. Lett.*, **97**, 255002  
 Oughton S., Dmitruk P., Matthaeus W. H., 2004, *Phys. Plasmas*, **11**, 2214  
 Parker E. N., 1957, *J. Geophys. Res.*, **62**, 509  
 Perez J. C., Mason J., Boldyrev S., Cattaneo F., 2012, *Phys. Rev. X*, **2**, 041005  
 Perez J. C., Mason J., Boldyrev S., Cattaneo F., 2014, *ApJ*, **793**, L13  
 Podesta J. J., 2009, *ApJ*, **698**, 986  
 Pucci F., Velli M., 2014, *ApJ*, **780**, L19  
 Rutherford P. H., 1973, *Phys. Fluids*, **16**, 1903  
 Samtaney R., Loureiro N. F., Uzdensky D. A., Schekochihin A. A., Cowley S. C., 2009, *Physical Review Letters*, **103**, 105004  
 Schekochihin A. A., Cowley S. C., Dorland W., Hammett G. W., Howes G. G., Quataert E., Tatsuno T., 2009, *ApJS*, **182**, 310  
 Shebalin J. V., Matthaeus W. H., Montgomery D., 1983, *J. Plasma Phys.*, **29**, 525  
 Strauss H. R., 1976, *Phys. Fluids*, **19**, 134  
 Sweet P. A., 1958, in Lehnert B., ed., *IAU Symposium Vol. 6, Electromagnetic Phenomena in Cosmical Physics*. p. 123  
 Tenerani A., Velli M., Pucci F., Landi S., Rappazzo A. F., 2016, *J. Plasma Phys.*, **82**, 535820501  
 Uzdensky D. A., Loureiro N. F., 2016, *Phys. Rev. Lett.*, **116**, 105003  
 Uzdensky D. A., Loureiro N. F., Schekochihin A. A., 2010, *Phys. Rev. Lett.*, **105**, 235002  
 Verdini A., Grappin R., 2015, *ApJ*, **808**, L34  
 Wicks R. T., Horbury T. S., Chen C. H. K., Schekochihin A. A., 2010, *MNRAS*, **407**, L31  
 Zhdarkin V., Boldyrev S., Uzdensky D. A., 2016, *Phys. Plasmas*, **23**, 055705